

# Image-based Geolocation by Ground-to-2.5D Map Matching

Mengjie Zhou  
University of Bristol  
Bristol, UK

mengjie.zhou@bristol.ac.uk

Liu Liu  
Huawei Cybaverse Lab  
Beijing, China

u1013337@anu.edu.au

Yiran Zhong  
Shanghai AI Lab  
Shanghai, China

zhongyiran@gmail.com

## Abstract

We study the image-based geolocation problem that aims to locate ground-view query images on cartographic maps. Previous methods often utilize cross-view localization techniques to match ground-view query images with 2D maps. However, the performance of these methods is frequently unsatisfactory due to the significant cross-view appearance differences. In this paper, we extend cross-view matching to 2.5D spaces, where the heights of the structures — such as trees, buildings, and other objects — can provide additional information to guide the cross-view matching. We present a new approach to learning representative embeddings from multi-modal data. Specifically, we first align 2D maps to ground-view panoramic images with polar transform to reduce the gap between panoramic images and maps. Then we leverage global fusion to fuse the multi-modal features from 2D and 2.5D maps to increase the distinctiveness of location embeddings. We construct the first large-scale ground-to-2.5D map geolocation dataset to validate our method and facilitate the research. We test our learned embeddings on two popular localization approaches, i.e., single-image based localization, and route based localization. Extensive experiments demonstrate that our proposed method achieves significantly higher localization accuracy and faster convergence than previous 2D map-based approaches.

## 1. Introduction

This paper studies the problem of image-based geolocation using ground-to-2.5D map matching. Given a ground-view query image, we aim to estimate the precise geospatial position where the query image was taken. This is done by querying the ground-view image with respect to a large-scale and georeferenced 2.5D map consisting of 2.5D structure models and 2D aerial-view map images. An example scenario of such a ground-to-2.5D map cross-view localization problem is illustrated in Figure 1.

Most state-of-the-art cross-view localization meth-

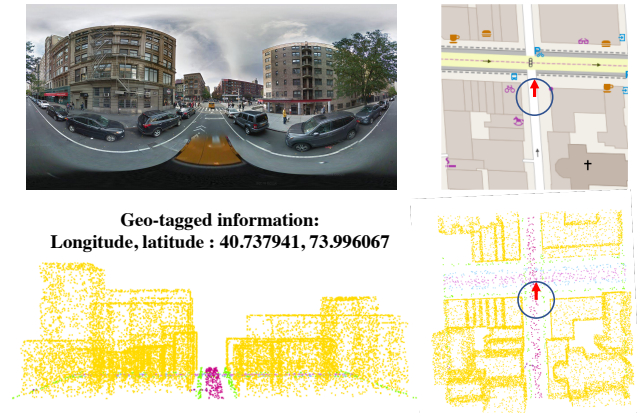


Figure 1. Illustration of query ground-view image and multi-modal map for the geolocation task. For the 2D map, the center of each map corresponds to the geo-tagged location, and the upward direction corresponds to the vehicle heading direction measured clockwise from north. The bottom two sub-figures show a 2.5D map viewed from different perspectives. The color is uniquely encoded by the semantic category.

ods [44, 10, 36, 37, 38, 17, 41, 48] employ a map with satellite/aerial RGB images for retrieval. Though effective, they have two principal limitations: i) The appearance of satellite map images changes with seasonal (summer, winter, etc.) and illumination (day, night, etc.) conditions. Furthermore, it also differs across satellites and covers dynamic objects such as cars and trees, bringing challenges for robust long-term localization; and ii) significant cross-view appearance differences. Since satellite view captures an image orthogonal to the ground plane, only the highest landmarks along the vertical direction are observable, whereas ground view can see the side views of these landmarks. The above-mentioned significant viewpoint difference presents significant challenges for matching cross-view images.

This paper addresses the two limitations mentioned above by using georeferenced 2.5D maps. We propose to use 2D maps as an alternative to satellite/aerial RGB images, as the 2D maps are both robust to time changes and compact. In addition, we include the height information of structures into the map to bridge the domain gap between

cross-view images, yielding the 2.5D model. Compared with detailed 3D models, the 2.5D model is compact and easy to achieve while still containing enough structure information for cross-view matching. It is worth noting that 2.5D maps are now enabled by the majority of mapping service providers, such as Google Maps and OpenStreetMap, and can be obtained easily.

Having both 2D maps and 2.5D structural models, how to learn discriminative feature embeddings for each multi-modal map to enable ground-view image retrieval? In this paper, we propose to fuse 2D maps and 2.5D structure models in the same feature space with a global fusion technique. Specifically, we first design a data processing pipeline to automatically extract 2.5D models from OpenStreetMap and convert them to the point cloud using the surface sampling strategy. Then we build a triplet-like architecture with InfoNCE loss [25] to learn an embedding space for intra- and inter-modal discrimination.

Ground-to-2.5D map geolocalization is a non-trivial task, *i.e.*, the significant difference in the appearance of panoramas and maps and the feature fusion between the image domain and the point cloud domain. To bridge the cross-view gap, we use the polar transform on 2D maps to coarsely align the geometric configuration between ground-view images and 2D maps. For multi-modal fusion, we analyze two fusion strategies, global fusion and local fusion, and find the global fusion achieves better performance.

To evaluate our method and facilitate the research, we constructed the first large-scale ground-to-2.5D map geolocalization dataset, which consists of 113767 panoramic images and geo-tagged maps from the cities of New York and Pittsburgh. There are three testing sets split for evaluation, each containing 5000 locations, covering trajectories of 69.3 km to 75.6 km. We perform two types of localization: single-image based localization and route based localization, using the extracted localization features to validate our method. Extensive experiments show that our multi-modal map based localization methods achieve higher localization accuracy than state-of-the-art methods [32]. In summary, the main contributions of this work are:

- A 2.5D map based cross-view localization method, enabling accurate long-term cross-view localization;
- A multi-modal feature extraction method, fusing features from 2D maps and 2.5D structure models;
- A large-scale 2.5D map based cross-view localization dataset, consisting of 113767 panoramic images and geo-tagged maps, densely covering multiple cities;
- State-of-the-art localization accuracy with two 2.5D map based cross-view localization methods: single-image based and route based localization methods, demonstrating the effectiveness of using 2.5D maps for cross-view localization.

## 2. Related Work

Image-based geolocalization has been extensively studied for years. There have been a significant number of papers published on this topic and we only cite some of the works that we consider most related to our method. We also briefly review some point-cloud processing methods for the sake of completeness.

**Cross-view Geolocalization** To tackle the data availability problem, using dense satellite imagery as the reference database has become an attractive geolocalization approach. The main challenge is feature extraction and similarity matching across views. Due to drastic appearance and viewpoint differences, traditional hand-crafted features obtain unsatisfactory performance [5, 15]. With the booming of deep learning, researchers begin to explore effective deep neural networks and efficient learning strategies for cross-view geolocalization. Efforts are mainly taken to develop task-related network layers [10, 36, 38, 37, 48], effective triplet loss [10, 41], large datasets [17], and geometric transformation to bridge the cross-view gap [17, 36].

**Map-related Task** Publicly available map data, such as OpenStreetMap (OSM), has been used for self-driving vehicles [7, 20, 35]. Inspired by the cross-view works, Panphattarasap and Calway [27] first proposed to use 2D OSM map as the reference database for the geolocalization task. To achieve high scalability, an extremely compact 4-bit descriptor indicating the presence or not of semantic features (junctions and building gaps) is designed to represent locations. Then, Samano et al. [32] generalized the approach in [27] by linking images to 2D maps in an embedding space. Not limited to the usage of 2D maps, researchers are also exploring the benefits of higher dimensional maps. Given an initial coarse estimate of location, Anil et al. [3] and Hai et al. [14] achieved global localization using 2.5D building maps.

**Point Cloud Representation Learning** The 2.5D map data is an untextured 3D map constructed from a 2D cadastral map with heights, which can be typically represented in the form of a point cloud. To directly process this irregular geometric data structure with neural networks, [29] first proposed a unified architecture named PointNet which is robust to the permutation variance of the point cloud input. However, PointNet treats each point independently and doesn't explore the local neighborhood information. Therefore, [30] proposed a hierarchical neural network named PointNet++ which applies PointNet [29] recursively on multiple point cloud subsets partitioned by metric space distance. Similarly, the method named DGCNN [46] also proposed to incorporate local neighboring information to enrich the representation power. The difference is that the DGCNN establishes the topological link of the neighborhood in feature space, rather than the metric space used in the PointNet++ [30]. It is indicated that the feature space can cap-

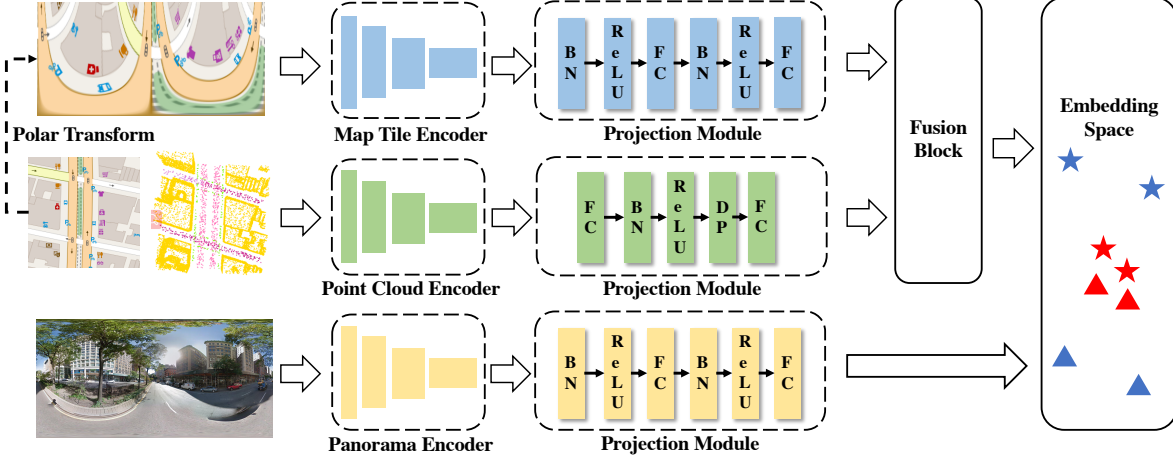


Figure 2. The overall network architecture consists of map tile branch, point cloud branch and panorama branch. Each branch is independent and contains a feature encoder and projection module. The 2D map tile is first projected to the polar coordinate system and then fused with features of 2.5D map for subsequent embedding space learning. In the embedding space, there are map embeddings (star) and image embeddings (triangle). The goal of the learning is to decrease the distance between positive pairs (red-to-red) while increase the distance between negative pairs (red-to-blue) in the embedding space.

ture semantic characteristics over potentially long distances. In recent years, self-attention networks have revolutionized natural language processing and image analysis. Motivated by this impressive development, [51] proposed the Point Transformer which introduces self-attention layers for point cloud representation learning. It is indicated that the self-attention operator is especially suitable for point cloud processing because of its permutation and cardinality invariance to the input elements.

### 3. Network Architecture

#### 3.1. Overall network architecture

The overall network architecture for learning location embeddings is illustrated in Figure 2. It is structured in a triplet-like shape with three individual branches, namely, Map Tile Branch, Point Cloud Branch, and Panorama Branch. The two upper branches are used to learn multi-modal map features and the bottom branch is used to learn semantic features from panoramic images. All learned features from various modalities are then fused for subsequent embedding space learning. It is worth noting that there is no weight sharing between branches because each one processes information that is vastly different from the others. In the following sections, we provide technical details of each branch and our feature fusion strategies.

#### 3.2. Map tile branch

The map tile branch is mainly used to extract features for the map tile input, which is an image of a local region of the 2D map. The map tile encoder is built upon the ResNet18 network [9], including four convolutional blocks to produce

a 512-channel feature volume with a resolution that is 1/32 of the original input. We use two fully connected layers preceded by batch normalization [12] and ReLU activation [24] to reduce the high dimension of the flattened feature to the desired embedding size.

Compared with satellite/aerial RGB images-based geolocalization, our map-based method not only has nearly orthogonal cross-view angles but also has significant appearance differences between ground view images and maps. To mitigate the cross-view discrepancy between ground-view and satellite/aerial images, previous methods often use explicit geometric transformation [36, 37, 42]. Since both map tiles and satellite images share the same viewing angle, we leverage a polar transformation to coarsely align the geometric configuration between the two views.

$$x_i^m = \frac{S_m}{2} - \frac{S_m}{2} \frac{(H_p - x_i^p)}{H_p} \cos\left(\frac{2\pi}{W_p} y_i^p\right) \quad (1)$$

$$y_i^m = \frac{S_m}{2} + \frac{S_m}{2} \frac{(H_p - x_i^p)}{H_p} \sin\left(\frac{2\pi}{W_p} y_i^p\right) \quad (2)$$

where  $(x_i^m, y_i^m)$  and  $(x_i^p, y_i^p)$  are pixel coordinates of original and polar transformed map tiles respectively. The height  $H_p$  of transformed images is the same as the size  $S_m$  of original maps.

As illustrated on the left side of Figure 2, the polar transformation closes the geometry domain gap between cross-view images and can help the network prioritize feature correspondence learning over geometric relationship learning.

#### 3.3. Point cloud branch

The 2.5D map we use is an untextured 3D map constructed from a 2D cadastral map augmented with height

information. The 2.5D structural model can be processed in a variety of ways. We use the point cloud form due to its simplicity and conducive to network processing.

We process the 2.5D map in the point cloud branch. The feature encoder is built upon popular backbones used for point cloud representation learning. In this paper, we study both MLP-based [29, 30, 46] and MLP-Transformer [51] based structure as the feature encode backbones and demonstrate the consistency of performance improvement brought by the 2.5D map. The projection module starts and ends with fully connected layers, and contains batch normalization, ReLU activation, and dropout layer [39] in the middle.

### 3.4. Multi-modal fusion

At the late stage of the map tile branch and point cloud branch, features from multi-modalities are fused for the subsequent embedding space learning. We study two fusion strategies, namely global fusion and local fusion.

**Global fusion** The global fusion works after the projection module. At this stage, the high  $C_h$ -channel feature volume including diverse local information has been aggregated into a lower  $C_l$ -channel feature vector. The multi-modal global feature vectors are first concatenated along the channel dimension and then projected to the desired embedding size after a fully connected layer.

**Local fusion** The local fusion operates before the projection module. At this stage, the feature volume  $\mathbf{F}_{2D}(H_f \times W_f \times C_{2D})$  and  $\mathbf{F}_{3D}(N \times C_{3D})$  have been extracted by map tile encoder and point cloud encoder, respectively. Refer to the method proposed in [16], we achieve the feature fusion at point-to-pixel level. Specifically, each point is first projected parallel to the 2D-image plane:

$$x_i = (\bar{x}_i + 0.5W_s - C_x) \frac{(W_f - 1)}{(W_s - 1)} \quad (3)$$

$$y_i = (\bar{y}_i + 0.5H_s - C_y) \frac{(H_f - 1)}{(H_s - 1)} \quad (4)$$

where  $(\bar{x}_i, \bar{y}_i)$  is the point coordinate, and  $(x_i, y_i)$  is the projected pixel coordinate.  $(W_f, H_f)$  and  $(W_s, H_s)$  are the size of the feature map in pixel and geographic level, respectively.  $N$  is the number of points. Then, the projected feature volume  $\bar{\mathbf{F}}_{2D}(N \times C_{2D})$  is generated by bilinear interpolation at  $(x, y)$  with the feature volume  $\mathbf{F}_{2D}$ , and concatenated with  $\mathbf{F}_{3D}$  after a multi-layer perceptron (MLP). Finally, after a max pooling and fully connected layer, the fused feature volume is processed to a fused global feature vector with the desired embedding size. For feature aggregation, max pooling as the symmetric function is suitable for processing the unordered point cloud data [29]. As indicated in [18], the low spatial resolution of the feature map affects the pixel-to-point knowledge transfer. Therefore, we use an extra transposed convolution after the map tile fea-

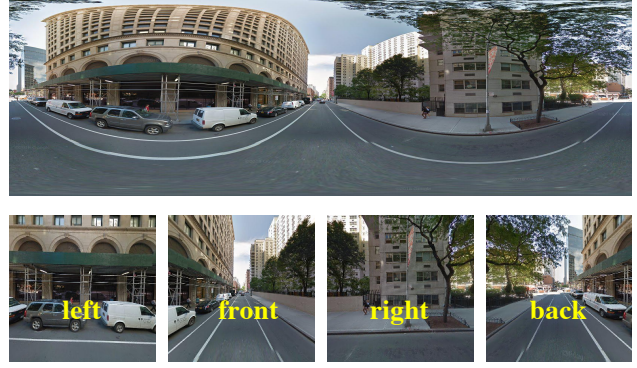


Figure 3. Illustration of a panoramic image (upper) and its four cropped snapshots (bottom) facing to the front, back, left and right.

ture encoder to expand the size of the feature map eight-fold to recover the spatial resolution.

### 3.5. Panorama branch

There are two ways to process the ground-view images. In [32], they crop the panorama images into four orthogonal views using Equirectangular Projection as shown in Figure 3. Although the angle of view as seen by a human is preserved in this method, the structural information of the scene, such as the height of the buildings, is compromised. Therefore, we choose to feed the original panorama directly into the panorama branch.

Because the content is more complex than map tiles, we use ResNet50 as the panorama encoder instead of ResNet18. In order to do a fair comparison with the previous single-modal method, we adopt the same architecture in the map tile and panorama branch as in [32]. We also use a projection module that is similar to the map tile branch to reduce the feature dimension to the desired embedding size.

## 4. Model Training

Our model is trained in an end-to-end way via contrastive learning. We combine intra-modal and inter-modal discrimination to formulate the loss function during training. As demonstrated in [11], richer data augmentation implies better generalization for contrastive self-supervised learning. Given an input panoramic image  $\mathbf{I}_i$ , we construct augmented versions  $\mathbf{I}_i^{t1}$  and  $\mathbf{I}_i^{t2}$  using transformations such as rotation, color jittering, normalization, erasing and Gaussian noising in sequence. Similarly, the augmented versions  $\mathbf{M}_i^{t1}$  and  $\mathbf{M}_i^{t2}$  of the map tile  $\mathbf{M}_i$  are constructed using transformations such as center cropping, normalization, erasing and Gaussian noising. For the point cloud  $\mathbf{P}_i$ ,  $\mathbf{P}_i^{t1}$  and  $\mathbf{P}_i^{t2}$  are constructed using rotation, translation, center cropping, jittering, and points removing in a sequential manner. All corresponding transformation parameters are generated randomly using uniform distribution in small

ranges to ensure positive alignment.

After the encoding and projection module, the global feature vectors of  $\mathbf{I}_i^{t_1}$  and  $\mathbf{I}_i^{t_2}$  are extracted which we denote as  $\mathbf{q}_i^{t_1}$  and  $\mathbf{q}_i^{t_2}$ . By using the fusion block, we get the fused global feature vector  $\mathbf{r}_i^{t_1}$  for  $(\mathbf{M}_i^{t_1}, \mathbf{P}_i^{t_1})$  and  $\mathbf{r}_i^{t_2}$  for  $(\mathbf{M}_i^{t_2}, \mathbf{P}_i^{t_2})$ . The optimization goal is to maximize the similarity of positive pairs while minimizing the similarity of negative pairs in a mini-batch. For the panorama-modal discrimination, the loss is calculated as:

$$\mathcal{L}_{pano} = \frac{1}{2N} \sum_{i=1}^N [l(\mathbf{q}_i^{t_1}, \mathbf{q}_i^{t_2}) + l(\mathbf{q}_i^{t_2}, \mathbf{q}_i^{t_1})] \quad (5)$$

The loss of the map-modal discrimination is calculated as:

$$\mathcal{L}_{map} = \frac{1}{2N} \sum_{i=1}^N [l(\mathbf{r}_i^{t_1}, \mathbf{r}_i^{t_2}) + l(\mathbf{r}_i^{t_2}, \mathbf{r}_i^{t_1})] \quad (6)$$

The loss of the cross-modal discrimination is calculated as:

$$\mathcal{L}_{cross} = \frac{1}{2N} \sum_{i=1}^N [l(\mathbf{q}_i, \mathbf{r}_i) + l(\mathbf{r}_i, \mathbf{q}_i)] \quad (7)$$

$$\mathbf{q}_i = \frac{1}{2}(\mathbf{q}_i^{t_1} + \mathbf{q}_i^{t_2}) \quad (8)$$

$$\mathbf{r}_i = \frac{1}{2}(\mathbf{r}_i^{t_1} + \mathbf{r}_i^{t_2}) \quad (9)$$

We leverage the InfoNCE loss [25] as the function of  $l(\mathbf{z}_i, \mathbf{h}_i)$  for the positive pair of  $\mathbf{z}_i$  and  $\mathbf{h}_i$ :

$$l(\mathbf{z}_i, \mathbf{h}_i) = -\log \frac{\exp(d(\mathbf{z}_i, \mathbf{h}_i)/\tau)}{\sum_{k=1}^N \exp(d(\mathbf{z}_i, \mathbf{h}_k)/\tau)} \quad (10)$$

where  $N$  is the mini-batch size (32 in this paper),  $\tau$  is the temperature co-efficient (0.07 in this paper), and  $d(\cdot)$  is the cosine similarity function, which executes the dot product between  $L_2$  normalized feature vector. Finally, the overall loss function is formulated as:

$$\mathcal{L} = \mathcal{L}_{pano} + \lambda_1 \mathcal{L}_{map} + \lambda_2 \mathcal{L}_{cross} \quad (11)$$

where  $\lambda_1$  and  $\lambda_2$  are weighting factors to control the influence of each loss component, which we set to be equal.

## 5. The Dataset

To evaluate our method and facilitate the research, we construct a large-scale ground-to-2.5D map geolocalization dataset. The ground-view images are collected from the StreetLearn Dataset [40, 23], consisting of 113767 panoramic images named with unique string identifiers in the cities of New York (Manhattan) and Pittsburgh. In the metadata, there is detailed information about the geographical position (lat/long coordinates and altitude in meters),

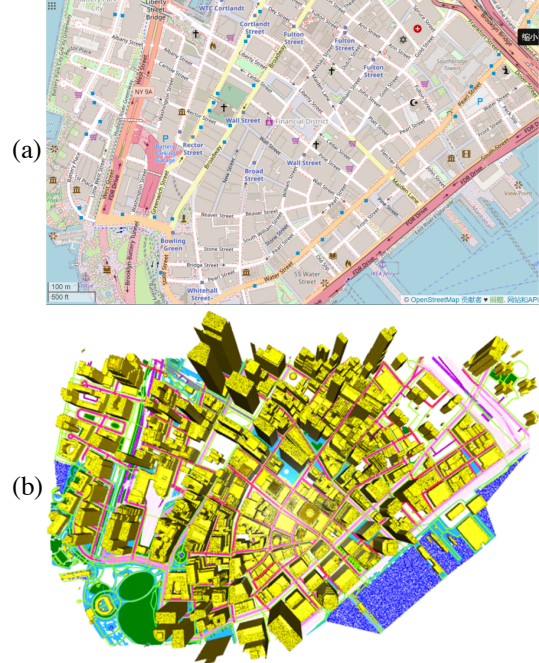


Figure 4. Multi-modal map dataset. The 2D and 2.5D maps from the partial area of Manhattan are respectively shown in (a) and (b). For the 2.5D map, the unique color is encoded by the semantic category.

camera orientation (pitch, roll, and yaw angles), and the connected neighbors of each location. To generate the training/testing/validation split, we use the same approach proposed in [32]. There are two testing sets from areas of Union Square and Wall Street, each containing 5000 locations, covering around 75.6 km and 73.1 km trajectories, respectively. The validation set is generated from the area of Hudson River with the same size as the testing set, covering around 69.3 km trajectory. There are diverse scenes in different areas, including skyscrapers, highways, parks, and riversides located on regular street grids (Union Square, Hudson River) or narrow streets with irregular intersections (Wall Street).

The multi-modal map data is automatically generated from the public map service, OpenStreetMap [26], as illustrated in Figure 4. The 2D map tiles with the size of  $256 \times 256$  are rendered using Mapnik [21]. Specifically, the center of each map tile corresponds to the geo-tagged location, and the upward direction of each map tile is aligned with the vehicle heading direction. We design a data processing pipeline to automatically process the 2.5D structure model from the OpenStreetMap (OSM) to the point cloud. Specifically, we first render the OSM metadata of each semantic category into a triangle-mesh structural model using Blender [6], then uniformly sample points on triangles using the Barycentric coordinate system [22]. The number of

points to be sampled is determined by the sampling density (0.1 in this paper) and surface area. Defining the vertices of a triangle as  $\mathbf{v}_1, \mathbf{v}_2, \mathbf{v}_3 \in R^3$ , the area is calculated as:

$$A = \frac{1}{2} \|(\mathbf{v}_1 - \mathbf{v}_3) \times (\mathbf{v}_2 - \mathbf{v}_3)\|_2 \quad (12)$$

And each new point  $\mathbf{p}$  is sampled as:

$$\mathbf{p} = (1 - \sqrt{r_1})\mathbf{v}_1 + \sqrt{r_1}(1 - r_2)\mathbf{v}_2 + \sqrt{r_1}r_2\mathbf{v}_3 \quad (13)$$

where  $r_1$  and  $r_2$  are two random variables uniformly distributed from 0 to 1. Finally, we merge points of each semantic category to a completed point cloud covering the whole area and crop the corresponding 2.5D map of a small region given the geo-tagged location. In this work, the multi-modal map data represent a local area with the size of  $152 \times 152 m^2$ . Totally, there are 98767 ground-view image and multi-modal map pairs for training, 5000 pairs for validation, and 10000 pairs for testing.

## 6. Experiments

### 6.1. Setting

We implement our network in Pytorch [28]. All models are trained in an end-to-end manner for 60 epochs on 4 Nvidia A100 80G GPUs. We empirically select ImageNet [8] pre-trained weights to initialize the map tile encoder and Places365 [52] for the panorama encoder. Both projection modules are initialized with normal distribution. For the multi-modal fusion module, the transposed convolution is initialized with bilinear kernels for the local fusion method. For the point cloud branch, the feature encoder and projection module are initialized with uniform distribution.

Before entering the network, the panorama and map tile is resized to  $448 \times 224$  and  $224 \times 224$  respectively. The dense point cloud is firstly normalized to the range of -1 to 1 and then downsampled to 1024 points with the farthest point sampling strategy. The embedding size is set to 128 or 16 for different localization methods. We use the Adam optimizer [13] with an initial learning rate  $4 \times 10^{-5}$  and weight decay  $1 \times 10^{-4}$ . The cosine annealing scheduler [19] is used to gradually decrease the learning rate to a minimum (0 in this paper). The model performing best on the validation set is chosen for the localization tasks.

### 6.2. Geolocalization results

We validate our learned location embeddings in two localization strategies, *i.e.*, single-image based localization and route based localization. For the former, we use the Top- $k$  recall rate to evaluate the geolocalization performance on the Hudson River, Wall Street, and Union Square. That is, given a query panoramic image, we retrieve the Top- $k$  geo-tagged reference maps by measuring the similarity ( $L_2$  distance) between their 128-D (Dimension) global

Model	HR-val	WS-test	US-test
ES	37.98/89.34	33.20/85.62	43.88/94.70
Ours-PointNet	46.82/91.58	42.36/89.74	55.08/96.90
Ours-PointNet++	47.10/92.88	42.17/90.03	52.52/96.92
Ours-DGCNN	<b>49.48/93.06</b>	<b>43.52/90.10</b>	<b>56.78/97.44</b>
Ours-PT	47.93/92.92	43.02/90.13	54.41/97.15

Table 1. Comparison between single-modal method and multi-modal methods. We use Embedding Space Descriptor (ES) [32] as the single-modal reference method. Various point cloud encoders are used to process 2.5D map data (marked with a suffix, PT is the abbrev Point Transformer). The Top-1/Top-1% recall rate is calculated to evaluate the localization performance in the area of Hudson River (HR, validation set), Wall Street (WS, test set), and Union Square (US, test set). The best results are shown in bold.

semantic features. If the matching reference map is ranked within the Top- $k$  list, a query panoramic image is considered to have been localized successfully. The Top- $k$  recall rate shows the percentage of correctly localized queries. For the latter, we use 500 randomly generated routes consisting of 40 adjacent locations in the area of Hudson River, Wall Street and Union Square. The test data is provided by work [32], and the distance between each location is around 10 meters. We adopt the Top-1 recall rate as our evaluation metric, which is measured by the percentage of correctly localized routes as a function of route length. Specifically, a route is considered to have been successfully localized at step  $t$  if and only if the matching reference maps from step  $t - 4$  to  $t$  are all ranked first.

**Single-image based localization** We present our quantitative results of single-image based localization in Table 1 with recorded Top-1/Top-1% recall rate. We include the state-of-the-art single-modal method [32] as a 2D map reference. We use global fusion as our multi-modal fusion strategy. The results demonstrate that using 2.5D maps can achieve significantly better performance than single-modal methods. We also compare the geolocalization performance with different point cloud backbones in Table 1. The best performance gains of 11.5%(Hudson River), 10.32%(Wall Street), and 12.9%(Union Square) are brought by using the DGCNN [46] as the point cloud encoder. We also illustrate examples of query panoramic images and the Top-5 retrieved maps in Figure 5. The corresponding map of each location image is outlined in red. The successful localization in these challenging environments indicates that our model has learned representative semantic features from both the panorama and map domains.

**Route based Localization** Route based localization is often used to localize in large areas, as a single descriptor is not sufficiently discriminative in large cities with a variety of repeated scene settings. We implement a route based localization method that is proposed in [27] with efficient

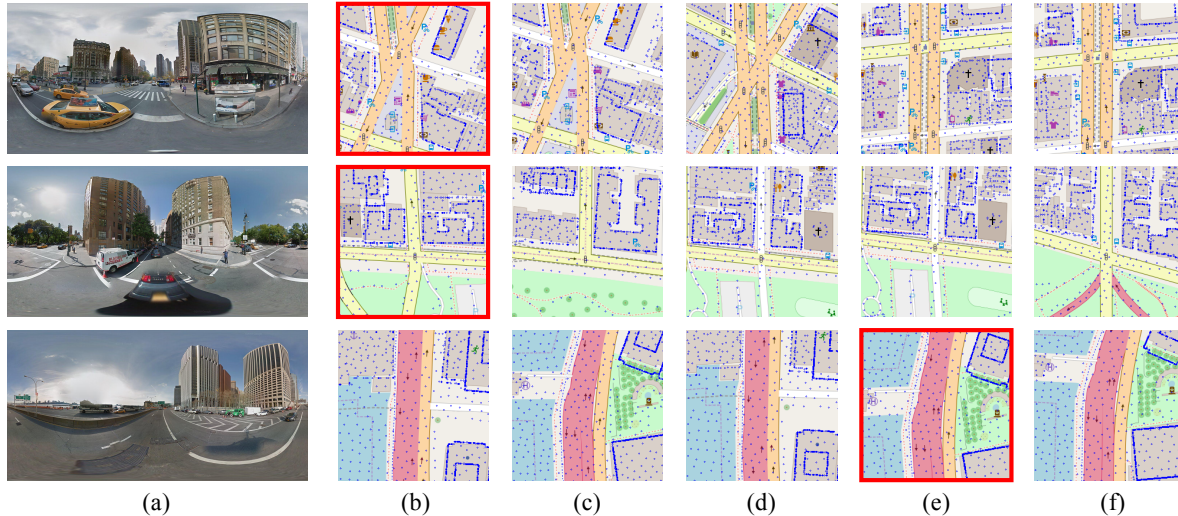


Figure 5. Top-5 retrieved maps (b)-(f) given a query panoramic image (a). The correct related map of the query is outlined in red.

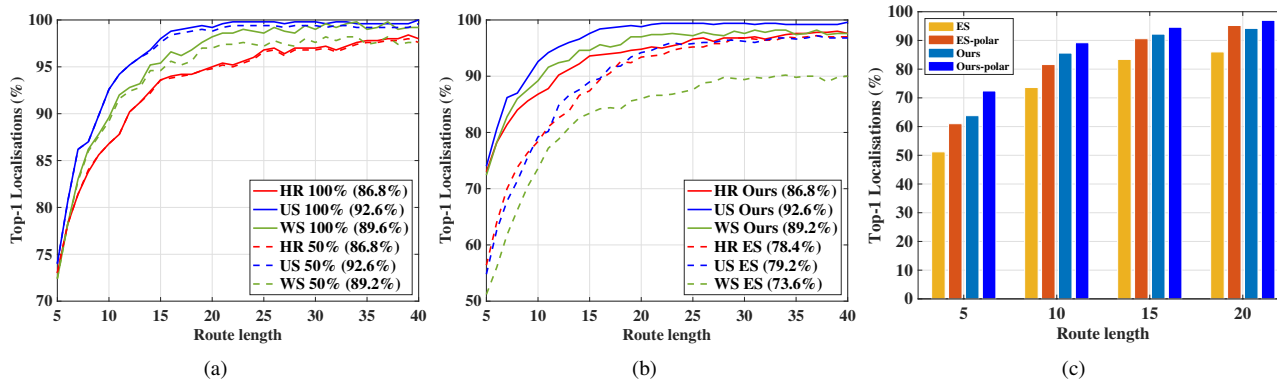


Figure 6. The performance of route based localization. (a) shows the comparison with and without the culling strategy. (b) shows the comparison between single-modal and multi-modal methods in three different areas. (c) shows the comparison between various map-based methods on Wall Street. HR, WS, and US separately represent the Hudson River, Wall Street, and Union Square. The Top-1 accuracy at step 10 is shown in the lower-right legend.

modifications, *i.e.*, rather than storing all route candidates in advance, we generate candidate routes online based on connectivity information between adjacent locations. To further improve the algorithm’s performance, we adopt a culling strategy to ensure localization efficiency.

Figure 6 (b) shows the performance of our method in route based localization. Compared with the state-of-the-art [32] in a single modal, our method achieves notably better performance. When moving to the location with a route length of 5, the multi-modal method already achieves over 70% localization accuracy, which is more than 15% higher than the single-modal method. The results indicate that the fusing of multi-modal map features for the route based localization task can achieve higher accuracy and faster convergence speed.

### 6.3. Ablation study

**Fusion strategy** There are two ways to fuse multi-modal features: global fusion and local fusion. Figure 7 illustrates the Top- $k\%$  recall rate localizing in Wall Street and Union Square, where  $k\%$  is the fraction of the dataset size. As shown, the global fusion has a 4.44% higher success rate than the local fusion in Wall Street and a 2.22% higher success rate in Union Square for Top-1 accuracy. The performance gap between these two fusion methods narrows as  $k$  increases. Since global fusion is simple and effective, we chose it as our feature fusion strategy.

**Polar transformation** As shown in Table 2, the polar transformation is beneficial to both single-modal and multi-modal methods. Compared with the single-modal method without polar transformation in single-image based localization, the multi-modal method with polar transformation

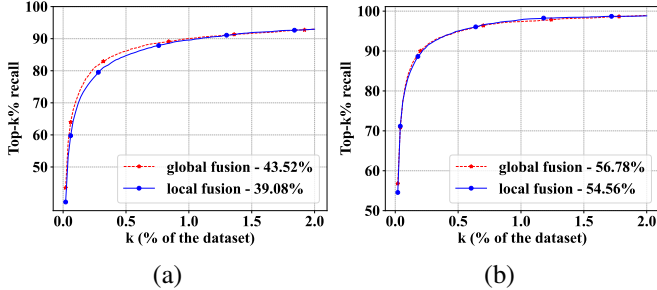


Figure 7. Comparison between multi-modal methods with local and global fusion in Wall Street(a) and Union Square(b). The Top-1 recall rate is presented in the lower-right legend.

Model	Pol	HR-val	WS-test	US-test
ES	-	37.98/89.34	33.20/85.62	43.88/94.70
ES	✓	45.06/90.74	38.74/87.28	51.42/96.62
Ours	-	49.48/93.06	43.52/90.10	56.78/97.44
Ours	✓	<b>51.86/93.26</b>	<b>47.66/91.20</b>	<b>63.18/98.44</b>

Table 2. Comparison between single-modal and multi-modal methods with and without polar transformation (Pol) in the area of Hudson River (HR-val), Wall Street (WS-test), and Union Square (US-test).

achieves 13.88%, 14.46%, and 19.3% gains in the localization performance on three different testing sets. Similar trends exist in route based localization. As shown in Figure 6 (c), the polar transformation can bring gains for both single-modal and multi-modal methods.

**Point sampling strategy** We compare two point cloud sampling strategies: farthest point sampling (FPS) and random point sampling (RPS). For each sampling strategy, we sample 512, 1024, and 2048 points for point cloud processing. As shown in Figure 8, using FPS generally has better localization accuracy, and more sampled points lead to better performance. It is probably because the FPS strategy preserves more structure information than RPS. We visualize the differences in Figure 9. Considering the trade-off between efficiency and accuracy, we chose an FPS of 1024 points as our sampling strategy.

**Embedding size** We explore the influence of the embedding size on single-image based localization. As shown in Table 3, there is a large performance degradation if we replace 128-D feature embeddings with 16-D embeddings. It indicates that low-dimensional representation is not sufficiently distinctive to allow localization with a single image.

**Culling strategy** To improve efficiency, we eliminate 50% of the route candidates at each movement until at least 100 remain. The impact of candidate culling on localization performance is shown in Figure 6(a). There is nearly no performance degradation in all testing areas. The results indicate that culling strategy is efficient while preserving the good localization capability. In addition, high similarity between

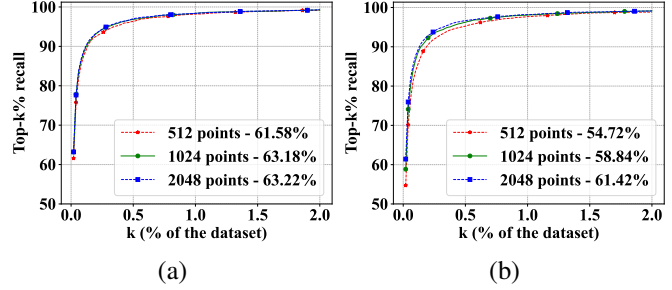


Figure 8. Robustness of multi-modal method to density variation and the number of points. Various types of point clouds are generated by the farthest point sampling (a) and random point sampling (b) in the area of Union Square. The Top-1 recall rate is presented in the lower-right legend.

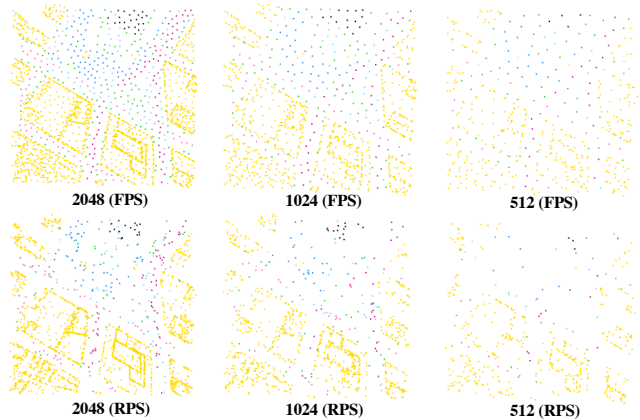


Figure 9. Point cloud data generated by farthest point sampling (FPS) and random point sampling (RPS). The color is uniquely encoded by the semantic category.

D	Pol	HR-val	WS-test	US-test
16	-	31.48/87.62	25.64/82.68	36.16/93.18
16	✓	37.12/89.06	30.42/83.38	41.28/95.60
128	-	49.48/93.06	43.52/90.10	56.78/97.44
128	✓	<b>51.86/93.26</b>	<b>47.66/91.20</b>	<b>63.18/98.44</b>

Table 3. Comparison between DGCNN-based multi-modal method using 16-D and 128-D semantic features with and without polar transformation (Pol) in the area of Hudson River (HR-val), Wall Street (WS-test) and Union Square (US-test).

curves also present that route discrimination occurs early and is maintained as routes growing, which leads to a faster and stable convergence. We adopt 50% culling approach for the route based localization task.

## 7. Conclusion

In this paper, we proposed ground-to-2.5D map matching for image-based geolocation. Unlike previous methods, which only used 2D maps as the georeferenced database, we extended the 2D maps to 2.5D maps, where



the heights of structures can be used to support cross-view matching. A new multi-modal representation learning framework is proposed to learn location embeddings from 2D images and point clouds. We also constructed the first large-scale ground-to-2.5D map geolocalization dataset to facilitate future research. Extensive experiments demonstrate that our multi-modal embeddings achieve significantly higher localization accuracy in both single-image based localization and route based localization.

## References

- [1] Mohamed Afham, Isuru Dissanayake, Dinithi Dissanayake, Amaya Dharmasiri, Kanchana Thilakarathna, and Ranga Rodrigo. Crosspoint: Self-supervised cross-modal contrastive learning for 3d point cloud understanding. In *Proceedings of the IEEE/CVF Conference on Computer Vision and Pattern Recognition*, pages 9902–9912, 2022.
- [2] Relja Arandjelovic, Petr Gronat, Akihiko Torii, Tomas Pajdla, and Josef Sivic. Netvlad: Cnn architecture for weakly supervised place recognition. In *Proceedings of the IEEE conference on computer vision and pattern recognition*, pages 5297–5307, 2016.
- [3] Anil Armagan, Martin Hirzer, Peter M. Roth, and Vincent Lepetit. Learning to align semantic segmentation and 2.5d maps for geolocalization. In *Proceedings of the IEEE Conference on Computer Vision and Pattern Recognition (CVPR)*, July 2017. 2
- [4] Clemens Arth, Christian Pirchheim, Jonathan Ventura, Dieter Schmalstieg, and Vincent Lepetit. Instant outdoor localization and slam initialization from 2.5 d maps. *IEEE Computer Architecture Letters*, 21(11):1309–1318, 2015.
- [5] Mayank Bansal, Harpreet S Sawhney, Hui Cheng, and Kostas Daniilidis. Geo-localization of street views with aerial image databases. In *Proceedings of the 19th ACM international conference on Multimedia*, pages 1125–1128, 2011. 2
- [6] Blender. 5
- [7] Marcus A Brubaker, Andreas Geiger, and Raquel Urtasun. Map-based probabilistic visual self-localization. *IEEE transactions on pattern analysis and machine intelligence*, 38(4):652–665, 2015. 2
- [8] Jia Deng, Wei Dong, Richard Socher, Li-Jia Li, Kai Li, and Li Fei-Fei. Imagenet: A large-scale hierarchical image database. In *Proc. IEEE Conf. on Computer Vision and Pattern Recognition*, 2009. 6
- [9] Kaiming He, Xiangyu Zhang, Shaoqing Ren, and Jian Sun. Deep residual learning for image recognition. In *Proceedings of the IEEE conference on computer vision and pattern recognition*, pages 770–778, 2016. 3
- [10] Sixing Hu, Mengdan Feng, Rang MH Nguyen, and Gim Hee Lee. Cvm-net: Cross-view matching network for image-based ground-to-aerial geo-localization. In *Proceedings of the IEEE Conference on Computer Vision and Pattern Recognition*, pages 7258–7267, 2018. 1, 2
- [11] Weiran Huang, Mingyang Yi, and Xuyang Zhao. Towards the generalization of contrastive self-supervised learning. *arXiv preprint arXiv:2111.00743*, 2021. 4
- [12] Sergey Ioffe and Christian Szegedy. Batch normalization: Accelerating deep network training by reducing internal covariate shift. In *International conference on machine learning*, pages 448–456. pmlr, 2015. 3
- [13] Diederik P Kingma and Jimmy Ba. Adam: A method for stochastic optimization. *arXiv preprint arXiv:1412.6980*, 2014. 6
- [14] Hai Li, Tianxing Fan, Hongjia Zhai, Zhaopeng Cui, Hujun Bao, and Guofeng Zhang. Bdloc: Global localization from 2.5d building map. In *International Symposium on Mixed and Augmented Reality/ISMAR*, pages 80–89. IEEE, 2021. 2
- [15] Tsung-Yi Lin, Serge Belongie, and James Hays. Cross-view image geolocalization. In *Proceedings of the IEEE Conference on Computer Vision and Pattern Recognition*, pages 891–898, 2013. 2
- [16] Haisong Liu, Tao Lu, Yihui Xu, Jia Liu, Wenjie Li, and Lijun Chen. Camliflow: bidirectional camera-lidar fusion for joint optical flow and scene flow estimation. In *Proceedings of the IEEE/CVF Conference on Computer Vision and Pattern Recognition*, pages 5791–5801, 2022. 4
- [17] Liu Liu and Hongdong Li. Lending orientation to neural networks for cross-view geo-localization. In *Proceedings of the IEEE/CVF Conference on Computer Vision and Pattern Recognition*, pages 5624–5633, 2019. 1, 2
- [18] Yueh-Cheng Liu, Yu-Kai Huang, Hung-Yueh Chiang, Hung-Ting Su, Zhe-Yu Liu, Chin-Tang Chen, Ching-Yu Tseng, and Winston H Hsu. Learning from 2d: Contrastive pixel-to-point knowledge transfer for 3d pretraining. *arXiv preprint arXiv:2104.04687*, 2021. 4
- [19] Ilya Loshchilov and Frank Hutter. Sgdr: Stochastic gradient descent with warm restarts. *arXiv preprint arXiv:1608.03983*, 2016. 6
- [20] Wei-Chiu Ma, Shenlong Wang, Marcus A Brubaker, Sanja Fidler, and Raquel Urtasun. Find your way by observing the sun and other semantic cues. In *2017 IEEE International Conference on Robotics and Automation (ICRA)*, pages 6292–6299. IEEE, 2017. 2
- [21] Mapnik. 5
- [22] Mark Meyer, Alan Barr, Haeyoung Lee, and Mathieu Desbrun. Generalized barycentric coordinates on irregular polygons. *Journal of graphics tools*, 7(1):13–22, 2002. 5
- [23] Piotr Mirowski, Andras Banki-Horvath, Keith Anderson, Denis Teplyashin, Karl Moritz Hermann, Mateusz Malinowski, Matthew Koichi Grimes, Karen Simonyan, Koray Kavukcuoglu, Andrew Zisserman, et al. The streetlearn environment and dataset. *arXiv:1903.01292*, 2019. 5
- [24] Vinod Nair and Geoffrey E Hinton. Rectified linear units improve restricted boltzmann machines. In *Proceedings of the 27th international conference on machine learning (ICML-10)*, pages 807–814, 2010. 3
- [25] Aaron van den Oord, Yazhe Li, and Oriol Vinyals. Representation learning with contrastive predictive coding. *arXiv preprint arXiv:1807.03748*, 2018. 2, 5
- [26] Open Street Map. 5
- [27] Pilailuck Panphattarasap and Andrew Calway. Automated map reading: Image based localisation in 2-d maps using binary semantic descriptors. In *2018 IEEE/RSJ International*

- Conference on Intelligent Robots and Systems (IROS)*, pages 6341–6348. IEEE, 2018. 2, 6
- [28] Adam Paszke, Sam Gross, Francisco Massa, Adam Lerer, James Bradbury, Gregory Chanan, Trevor Killeen, Zeming Lin, Natalia Gimelshein, Luca Antiga, et al. Pytorch: An imperative style, high-performance deep learning library. *Advances in neural information processing systems*, 32, 2019. 6
- [29] Charles R Qi, Hao Su, Kaichun Mo, and Leonidas J Guibas. Pointnet: Deep learning on point sets for 3d classification and segmentation. In *Proceedings of the IEEE conference on computer vision and pattern recognition*, pages 652–660, 2017. 2, 4
- [30] Charles Ruizhongtai Qi, Li Yi, Hao Su, and Leonidas J Guibas. Pointnet++: Deep hierarchical feature learning on point sets in a metric space. *Advances in neural information processing systems*, 30, 2017. 2, 4
- [31] Krishna Regmi and Mubarak Shah. Bridging the domain gap for ground-to-aerial image matching. In *Proceedings of the IEEE/CVF International Conference on Computer Vision*, pages 470–479, 2019.
- [32] Noe Samano, Mengjie Zhou, and Andrew Calway. You are here: Geolocation by embedding maps and images. In *European Conference on Computer Vision*, pages 502–518. Springer, 2020. 2, 4, 5, 6, 7
- [33] Torsten Sattler, Michal Havlena, Konrad Schindler, and Marc Pollefeys. Large-scale location recognition and the geometric burstiness problem. In *Proceedings of the IEEE Conference on Computer Vision and Pattern Recognition*, pages 1582–1590, 2016.
- [34] Grant Schindler, Matthew Brown, and Richard Szeliski. City-scale location recognition. In *2007 IEEE Conference on Computer Vision and Pattern Recognition*, pages 1–7. IEEE, 2007.
- [35] Ari Seff and Jianxiong Xiao. Learning from maps: Visual common sense for autonomous driving. *CoRR*, abs/1611.08583, 2016. 2
- [36] Yujiao Shi, Liu Liu, Xin Yu, and Hongdong Li. Spatial-aware feature aggregation for image based cross-view geo-localization. *Advances in Neural Information Processing Systems*, 32:10090–10100, 2019. 1, 2, 3
- [37] Yujiao Shi, Xin Yu, Dylan Campbell, and Hongdong Li. Where am i looking at? joint location and orientation estimation by cross-view matching. In *Proceedings of the IEEE/CVF Conference on Computer Vision and Pattern Recognition*, pages 4064–4072, 2020. 1, 2, 3
- [38] Yujiao Shi, Xin Yu, Liu Liu, Tong Zhang, and Hongdong Li. Optimal feature transport for cross-view image geo-localization. In *Proceedings of the AAAI Conference on Artificial Intelligence*, volume 34, pages 11990–11997, 2020. 1, 2
- [39] Nitish Srivastava, Geoffrey Hinton, Alex Krizhevsky, Ilya Sutskever, and Ruslan Salakhutdinov. Dropout: a simple way to prevent neural networks from overfitting. *The journal of machine learning research*, 15(1):1929–1958, 2014. 4
- [40] StreetLearn. 5
- [41] Bin Sun, Chen Chen, Yingying Zhu, and Jianmin Jiang. Geocapsnet: Ground to aerial view image geo-localization using capsule network. In *2019 IEEE International Conference on Multimedia and Expo (ICME)*, pages 742–747. IEEE, 2019. 1, 2
- [42] Aysim Toker, Qunjie Zhou, Maxim Maximov, and Laura Leal-Taixé. Coming down to earth: Satellite-to-street view synthesis for geo-localization. In *Proceedings of the IEEE/CVF Conference on Computer Vision and Pattern Recognition*, pages 6488–6497, 2021. 3
- [43] Akihiko Torii, Relja Arandjelovic, Josef Sivic, Masatoshi Okutomi, and Tomas Pajdla. 24/7 place recognition by view synthesis. In *Proceedings of the IEEE Conference on Computer Vision and Pattern Recognition*, pages 1808–1817, 2015.
- [44] Nam N Vo and James Hays. Localizing and orienting street views using overhead imagery. In *European conference on computer vision*, pages 494–509. Springer, 2016. 1
- [45] Tomas Vojir, Ignas Budvytis, and Roberto Cipolla. Efficient large-scale semantic visual localization in 2d maps. In *Proceedings of the Asian Conference on Computer Vision*, 2020.
- [46] Yue Wang, Yongbin Sun, Ziwei Liu, Sanjay E Sarma, Michael M Bronstein, and Justin M Solomon. Dynamic graph cnn for learning on point clouds. *Acm Transactions On Graphics (tog)*, 38(5):1–12, 2019. 2, 4, 6
- [47] Fan Yan, Olga Vysotska, and Cyrill Stachniss. Global localization on openstreetmap using 4-bit semantic descriptors. In *2019 European Conference on Mobile Robots (ECMR)*, pages 1–7. IEEE, 2019.
- [48] Hongji Yang, Xiufan Lu, and Yingying Zhu. Cross-view geo-localization with layer-to-layer transformer. In M. Ranzato, A. Beygelzimer, Y. Dauphin, P.S. Liang, and J. Wortman Vaughan, editors, *Advances in Neural Information Processing Systems*, volume 34, pages 29009–29020, 2021. 1, 2
- [49] Amir Roshan Zamir and Mubarak Shah. Accurate image localization based on google maps street view. In *European Conference on Computer Vision*, pages 255–268. Springer, 2010.
- [50] Amir Roshan Zamir and Mubarak Shah. Image geo-localization based on multiplenearest neighbor feature matching using generalized graphs. *IEEE transactions on pattern analysis and machine intelligence*, 36(8):1546–1558, 2014.
- [51] Hengshuang Zhao, Li Jiang, Jiaya Jia, Philip HS Torr, and Vladlen Koltun. Point transformer. In *Proceedings of the IEEE/CVF international conference on computer vision*, pages 16259–16268, 2021. 3, 4
- [52] Bolei Zhou, Agata Lapedriza, Aditya Khosla, Aude Oliva, and Antonio Torralba. Places: A 10 million image database for scene recognition. *IEEE Trans on Pattern Analysis and Machine Intelligence*, 40(6):1452–1464, 2017. 6